Celestial Mech Dyn Astr (2008) 100:63–91
DOI 10.1007/s10569-007-9108-3

ORIGINAL ARTICLE

Energy and stability in the Full Two Body Problem

Julie Bellerose · Daniel J. Scheeres

Received: 31 July 2007 / Revised: 16 September 2007 / Accepted: 19 November 2007 /
Published online: 18 December 2007

Abstract The conditions for relative equilibria and their stability in the Full Two Body Problem are derived for an ellipsoid–sphere system. Under constant angular momentum it is found that at most two solutions exist for the long-axis solutions with the closer solution being unstable while the other one is stable. As the non-equilibrium problem is more common in nature, we look at periodic orbits in the F2BP close to the relative equilibrium conditions. Families of periodic orbits can be computed where the minimum energy state of one family is the relative equilibrium state. We give results on the relative equilibria, periodic orbits and dynamics that may allow transition from the unstable configuration to a stable one via energy dissipation.

Keywords Full Two-Body Problem · Ellipsoid–sphere system · Relative equilibria · Stability · Periodic orbits

Mathematics Subject Classification (2000) 70505

1 Introduction

Over the past few decades, we witnessed a growing interest in studying small bodies of our solar system. Some studies have indicated that about 16% of the Near-Earth Asteroids may be systems of asteroid pairs, or binary asteroid systems (Margot et al. 2002). The problem formulation of the binary system itself has been posed and studied in earlier work, see Maciejewski (1995), Scheeres (2003, 2006), Scheeres and Augenstein (2003), Fahnestock and Scheeres (2006), Lee et al. (2007), Scheeres and Bellerose (2005), and Bellerose and Scheeres (2007b). As the mass distribution of the bodies is considered, the problem is referred to as the Full Two Body Problem (F2BP). Assuming a general formulation is possible (Maciejewski 1995; Scheeres 2006). Fahnestock and Scheeres (2006) approached the problem using polyhedral mutual potential and potential derivatives while other studies have used other mathematical methods such as Lie group computations (Lee et al. 2007).

J. Bellerose (✉) · D. J. Scheeres
University of Michigan, 1320 Beal Ave., Ann Arbor, MI 48109-2140, USA
e-mail: juliebel@umich.edu

The conditions for relative equilibria and their stability in the F2BP are derived for a system with one of the bodies being a sphere while the other one is of arbitrary shape (Scheeres 2006). An ellipsoid–sphere system was further investigated (Scheeres 2003; Scheeres and Augenstein 2003) and equilibrium solutions and their stability for a spacecraft in this gravitational field have also been studied (Scheeres and Bellerose 2005; Bellerose and Scheeres 2007b).

In the first part of the current work, we investigate cases of relative equilibria for an ellipsoid–sphere system under constant angular momentum. For convenience, we will refer to this problem as the F2BP. We show existence and stability properties of these solutions and give some results. We also look briefly at relative equilibria for different values of angular momentum and give a short discussion on how these can be linked to the formation and evolution of a binary system.

As the non-equilibrium problem is more common in nature, studies have looked at periodic orbits in the F2BP for an ellipsoid–sphere system (Bellerose and Scheeres 2005, 2007a). As a first approximation, the motion of the binary system was set as constant, where the ratio of the angular spin of the general body to their system orbit rate was a free parameter. Although useful for computations, this approximation allows systems that do not exist in nature. In the present work, we solve for the real dynamics of the F2BP under non-equilibrium condition. We can show existence of periodic orbits near relative equilibria where the stability of the periodic orbits follows the relative equilibria stability properties. We also link these two topics through energy consideration; for a family of periodic orbits, relative equilibrium parameters give the minimum energy state for this family.

For computing periodic orbits, it is more convenient to choose a frame fixed to the general body as this permits us to eliminate its attitude dynamics from consideration. We define a surface normal to the flow and integrate the system until it crosses the surface of section. Using this approach, we can converge on symmetric periodic orbits after correcting the initial states and iterating until the difference between the initial and final state is small. By linearizing the system near relative equilibria, an approximation method is also derived in order to facilitate the computation and use of periodic orbits near relative equilibria.

2 The Full Two-Body Problem

2.1 Geometry of the problem and equations of motion

The Two-Body Problem considers the dynamics of two spherical bodies in orbit about each other. We refer to the Full Two-Body Problem (F2BP) when we consider the mass distribution of at least one of the two bodies. The general situation is shown in Fig. 1a. Without any approximations, this system involves 12 degrees of freedom. The sphere restriction shown in Fig. 1b reduces the problem to lower dimension. In total, six degrees of freedom can be removed from the conservation of angular momentum and the rotational dynamics of the sphere while keeping the interesting dynamical features (Scheeres 2006).

In the current work, we study the dynamics of an ellipsoid–sphere system, and refer to it as the F2BP. In Fig. 2, we define M_1 and M_2 as the masses of the spherical and ellipsoidal shapes, respectively, with a mass fraction defined as

$$\nu = \frac{M_1}{M_1 + M_2}. \tag{1}$$

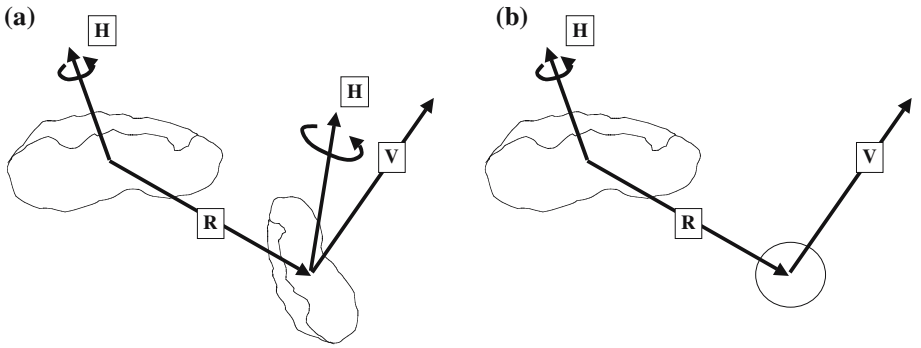

Fig. 1 (**a**) Restricted Full 2-Body Problem (F2BP). (**b**) F2BP under "Sphere Restriction"

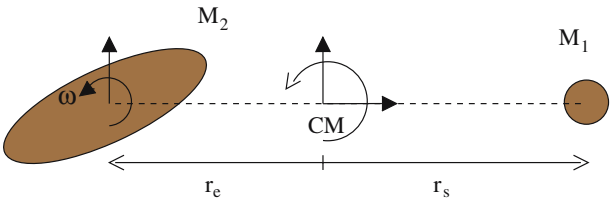

Fig. 2 F2BP: geometry of the problem

In dimensional form, the position of the two bodies relative to their center of mass are

$$\boldsymbol{r_e} = -\nu \boldsymbol{r_b} \tag{2}$$

and

$$\boldsymbol{r_s} = (1-\nu)\boldsymbol{r_b}, \tag{3}$$

where subscripts e and s refer to the ellipsoid and the spherical body, respectively, and $\boldsymbol{r_b}$ is the position vector of the sphere relative to the ellipsoid. For a rotating coordinate frame fixed to the ellipsoidal body, the two bodies' relative dynamics are defined by

$$\ddot{\boldsymbol{r_b}} + 2\boldsymbol{\Omega} \times \dot{\boldsymbol{r_b}} + \dot{\boldsymbol{\Omega}} \times \boldsymbol{r_b} + \boldsymbol{\Omega} \times (\boldsymbol{\Omega} \times \boldsymbol{r_b}) = G(M_1 + M_2)\frac{\partial \tilde{U}}{\partial \boldsymbol{r_b}} \tag{4}$$

and the rotational dynamics of the ellipsoid are described by

$$\hat{\boldsymbol{I}} \cdot \dot{\boldsymbol{\Omega}} + \boldsymbol{\Omega} \times \hat{\boldsymbol{I}} \cdot \boldsymbol{\Omega} = -GM_1 \boldsymbol{r_b} \times \frac{\partial \tilde{U}}{\partial \boldsymbol{r_b}}, \tag{5}$$

where $\boldsymbol{\Omega}$ is the angular velocity of the ellipsoid and $\hat{\boldsymbol{I}}$ is its inertia matrix normalized by its mass (Scheeres 1998). In the general case, $\tilde{U}$ is the mutual potential, defined as

$$\tilde{U} = \frac{1}{M_2}\int_{\beta_2} \frac{dm_2(\hat{\boldsymbol{\rho}})}{|\boldsymbol{r_b} + \hat{\boldsymbol{\rho}}|}, \tag{6}$$

where $\hat{\rho}$ is the position vector of a mass element of the ellipsoid. Note that, since the frame is fixed to the ellipsoidal body, the mutual potential is time-invariant. This is true independent of whether the system is in relative equilibrium.

To simplify the computation, the maximum radius of the ellipsoid, α, and the mean motion of the system at this radius, $n = \sqrt{G(M_1 + M_2)/\alpha^3}$, are chosen as length and time scales, respectively. Let $\boldsymbol{\omega}$ be the normalized angular velocity of the ellipsoid.

As derived in (Scheeres 1998), in Lagrangian form the F2BP dynamics can be written as follows

$$\ddot{\boldsymbol{r}} + 2\boldsymbol{\omega} \times \dot{\boldsymbol{r}} + \dot{\boldsymbol{\omega}} \times \boldsymbol{r} + \boldsymbol{\omega} \times (\boldsymbol{\omega} \times \boldsymbol{r}) = \frac{\partial U}{\partial \boldsymbol{r}} \tag{7}$$

and

$$\boldsymbol{I} \cdot \dot{\boldsymbol{\omega}} + \boldsymbol{\omega} \times \boldsymbol{I} \cdot \boldsymbol{\omega} = -\nu \boldsymbol{r} \times \frac{\partial U}{\partial \boldsymbol{r}}. \tag{8}$$

Using the normalized units, the mutual potential, U, and the inertia matrix of the general body, $\boldsymbol{I}$, are expressed as

$$U = \frac{\alpha}{M_2} \int_{\beta_e} \frac{dm(\boldsymbol{\rho})}{|\boldsymbol{r} + \boldsymbol{\rho}|} \tag{9}$$

and

$$\boldsymbol{I} = -\frac{1}{M_2 \alpha^2} \int_{\beta_e} \tilde{\boldsymbol{\rho}} \cdot \tilde{\boldsymbol{\rho}} dm, \tag{10}$$

where $\boldsymbol{\rho}$ is the position vector of a mass element of the distributed body. Note that $\tilde{(\cdot)}$ represents the cross-product matrix.

Since we model the general body as an ellipsoid, the mutual potential, U, can be written in terms of elliptic integrals (Danby 1992). We use the normalization above to express

$$U = \frac{3}{4} \int_{\lambda}^{\infty} \phi(\boldsymbol{r}, v) \frac{dv}{\Delta(v)} \tag{11}$$

with

$$\phi(\boldsymbol{r}, v) = 1 - \frac{(x + \nu r)^2}{1 + v} - \frac{y^2}{\beta^2 + v} - \frac{z^2}{\gamma^2 + v} \tag{12}$$

and

$$\Delta(v) = \sqrt{(1 + v)(\beta^2 + v)(\gamma^2 + v)}, \tag{13}$$

where $0 < \gamma \leq \beta \leq 1$, γ and β correspond to the z and y radii of the ellipsoid, and λ satisfies $\phi(\boldsymbol{r}, \lambda) = 0$.

In the $x - y$ plane, the Lagrange form of the equations of motion is given by Eqs. (7, 8), where

$$\dot{\omega} = -\frac{\nu}{I_{zz}} \left(x \frac{\partial U}{\partial y} - y \frac{\partial U}{\partial x} \right), \tag{14}$$

$$\ddot{x} = \omega^2 x + 2\omega \dot{y} + \dot{\omega} y + \frac{\partial U}{\partial x}, \tag{15}$$

and

$$\ddot{y} = \omega^2 y - 2\omega \dot{x} - \dot{\omega} x + \frac{\partial U}{\partial y}. \tag{16}$$

When considering planar motion, this model also allows us to write the system as a two degree of freedom Hamiltonian system. The position of the sphere relative to the ellipsoid in the plane is denoted as $\boldsymbol{q} = \boldsymbol{r}$, and the inertial velocity is, $\boldsymbol{p} = \dot{\boldsymbol{r}} + \boldsymbol{\omega} \times \boldsymbol{r}$. Using this set of coordinates, we can write the energy and momentum integrals in normalized units as

$$E = \frac{1}{2} \boldsymbol{p} \cdot \boldsymbol{p} + \frac{1}{2\nu} I_{zz} \omega^2 - U(\boldsymbol{q}) \tag{17}$$

and

$$K = \frac{1}{\nu} I_{zz}\omega + \hat{z} \cdot (\boldsymbol{q} \times \boldsymbol{p}). \tag{18}$$

We can solve for the rotation rate ω as function of K, $\boldsymbol{q}$ and $\boldsymbol{p}$.

$$\omega = \frac{\nu}{I_{zz}} \left[K - \hat{z} \cdot (\boldsymbol{q} \times \boldsymbol{p}) \right]. \tag{19}$$

Hence, for given values of K, $\boldsymbol{q}$ and $\boldsymbol{p}$, we can substitute for ω into the energy equation, Eq. (17)

$$E = \frac{1}{2}\boldsymbol{p} \cdot \boldsymbol{p} + \frac{\nu}{2I_{zz}} \left[K - \hat{z} \cdot (\boldsymbol{q} \times \boldsymbol{p}) \right]^2 - U(\boldsymbol{q}). \tag{20}$$

Note that in this case, the energy integral is the Hamiltonian, or $E = H(\boldsymbol{q}, \boldsymbol{p})$ with angular momentum K as a free parameter. For general three dimensional motion the angular momentum cannot be eliminated in the same way, as its elimination would couple the relative attitude of the body into the energy (Scheeres 2006). In explicit form for planar motion, Eq. (20) becomes

$$H(q_x, q_y, p_x, p_y) = \frac{1}{2}({p_x}^2 + {p_y}^2) + \frac{\nu}{2I_{zz}} \left[K - (q_x p_y - p_x q_y) \right]^2 - U(q_x, q_y). \tag{21}$$

We can compute the dynamics with

$$\dot{q_x} = H_{p_x} = p_x + q_y \frac{\nu}{I_{zz}} \left[K - (q_x p_y - p_x q_y) \right], \tag{22}$$

$$\dot{q_y} = H_{p_y} = p_y - q_x \frac{\nu}{I_{zz}} \left[K - (q_x p_y - p_x q_y) \right], \tag{23}$$

$$\dot{p_x} = -H_{q_x} = p_y \frac{\nu}{I_{zz}} \left[K - (q_x p_y - p_x q_y) \right] + \frac{\partial U}{\partial q_x}, \tag{24}$$

and

$$\dot{p_y} = -H_{q_y} = -p_x \frac{\nu}{I_{zz}} \left[K - (q_x p_y - p_x q_y) \right] + \frac{\partial U}{\partial q_y}, \tag{25}$$

where the subscripts denote partial differentiation.

2.2 Relative equilibria for an ellipsoid–sphere system

A particular solution of the F2BP is for the two bodies to be in relative equilibrium. Relative equilibrium conditions are found by setting all velocities and accelerations to zero in Eqs. (7, 8) or setting all time derivatives to zero in Eqs. (22–25). In the general case, this involves six equations to solve for the position and angular velocity components or six for position and momentum. Previous studies have looked at relative equilibria for arbitrary mass distribution (Scheeres 2006). For the case of symmetry assumption on the gravitational potential, Scheeres (2003) and Scheeres and Augenstein (2003) provide a discussion of the properties of relative equilibrium in the F2BP and their stability. Note that only the planar case is considered here.

Now consider the Hamiltonian system with an equilibrium solution where the two bodies are aligned along the x-axis

$$\boldsymbol{q} = [q, 0]^T \tag{26}$$

and

$$\boldsymbol{p} = [0, p]^T. \tag{27}$$

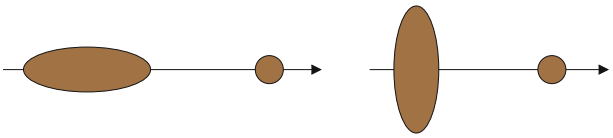

Fig. 3 Configurations investigated for the Full Two-Body Problem

We solve for q with $\dot{\boldsymbol{q}} = \dot{\boldsymbol{p}} = 0$ in Eqs. (23, 24) and obtain

$$1 = \frac{\nu q}{I_{zz} p} [K - qp] \tag{28}$$

and

$$I(q) = \frac{\nu p}{I_{zz} q} [K - qp], \tag{29}$$

where we express $\frac{\partial U}{\partial q_x} = \frac{\partial U}{\partial q} = -I(q)\boldsymbol{q}$, with

$$I(q) = \frac{3}{2} \int_{\lambda}^{\infty} \frac{du}{(u+1)\triangle(u)} \tag{30}$$

and $\lambda = q^2 - \alpha^2$. Note that $\hat{\mathbf{z}} \cdot (\boldsymbol{q} \times \boldsymbol{p}) = qp$. From Eq. (28), we express

$$p = \frac{(\nu q K / I_{zz})}{\left(1 + \nu q^2 / I_{zz}\right)}, \tag{31}$$

and substitute p in Eq. (29) to get

$$I(q) = \frac{(\nu K / I_{zz})^2}{\left(1 + \nu q^2 / I_{zz}\right)^2}. \tag{32}$$

Given values of angular momentum, mass ratio and ellipsoidal parameters, we solve for the possible distances between the bodies, q, for which the system is in relative equilibrium. For the case of an ellipsoid–sphere system, two configurations exist: with the minimum moment of inertia aligned with the axis joining the two bodies and where it is perpendicular to it. The two cases are shown on Fig. 3. In the present work, we only consider the long-axis case as only it can have energetically stable solutions (Scheeres 2003).

Previous work has mapped these relative equilibria solutions as a function of the mass ratio, also characterizing their stability and energy properties (Scheeres 2003). Figure 4 shows results for an ellipsoid with semi-major axes of $\alpha = 1$, $\beta = 0.5$ and $\gamma = 0.25$. On this plot, every point is a relative equilibrium and the shaded region indicates the transition between stable and unstable equilibrium. The solid line represents the transition from negative to positive total energy of the system, i.e., $E = 0$. This indicates the capability of the binary system to evolve into an escaping system with sufficient perturbation (possible for $E > 0$). Finally the pointed dashed line indicates the distance between the bodies when resting on each other assuming they have the same density. Note that each such relative equilibrium in Fig. 4 corresponds to a different value of angular momentum in general.

As a binary system will most likely lose energy through internal dissipation and conserve angular momentum (see Scheeres et al. (2006) for a case study of 1999 KW4), we are interested in studying its dynamics under constant angular momentum. For a given value of angular momentum and a value for the system mass ratio in Eq. (32), we can solve for at most

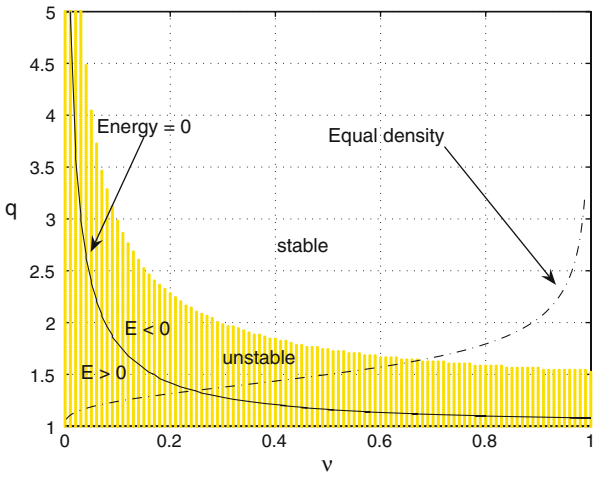

Fig. 4 Stability diagram for planar motion in the long-axis solution. The clear region denotes spectral stability while the shaded one denotes a single hyperbolic manifold instability. The solid line indicates transition from positive to negative total energy of the system and the pointed dashed line assumes equal density of the binary bodies. Parameters are $\alpha = 1$, $\beta = 0.5$, $\gamma = 0.25$ (Scheeres 2003)

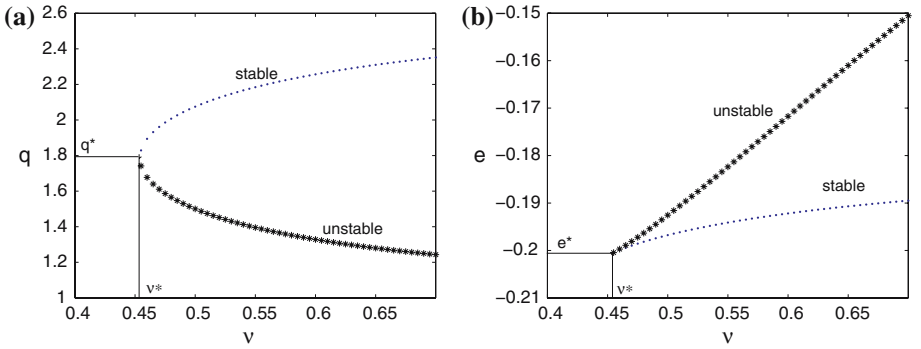

Fig. 5 System with angular momentum, $K = 1.715$ (nondimensional), and ellipsoidal shape parameters $\gamma = \frac{1}{2}\beta = 0.5$. (**a**) Locus of solutions q as function of the mass ratio, for a constant angular momentum. The upper and lower branches represent stable and unstable solutions, respectively. (**b**) Energy plot of relative equilibrium solutions as function of the mass ratio ν, with constant angular momentum. The lower and upper branches represent unstable and stable solutions, respectively

two relative equilibria, shown on Fig. 5a. We refer to the second solution as the conjugate solution. There is one single solution, or bifurcation value, at the mass ratio, ν^*, and solution q^*, which is at the left end of the U-shaped curve on Fig. 5a. For $\nu > \nu^*$, the system has two relative equilibrium solutions. Figure 5b represents the energy associated with the relative equilibria of Fig. 5a; the upper and lower branches in (b) correspond to the lower and upper branches in (a), respectively. It is clear that a system in the closer equilibrium configuration has more energy. For the case of two solutions, in the next section we show that at a given mass ratio ν the closer equilibrium is always unstable while its conjugate solution is always stable.

We define the "free energy" as

$$\Delta E = E_{URE} - E_{SRE}, \tag{33}$$

where E_{URE} is the energy at the unstable configuration and E_{SRE} is the one at the stable equilibrium, which is also the minimum energy state. A binary system can be at a

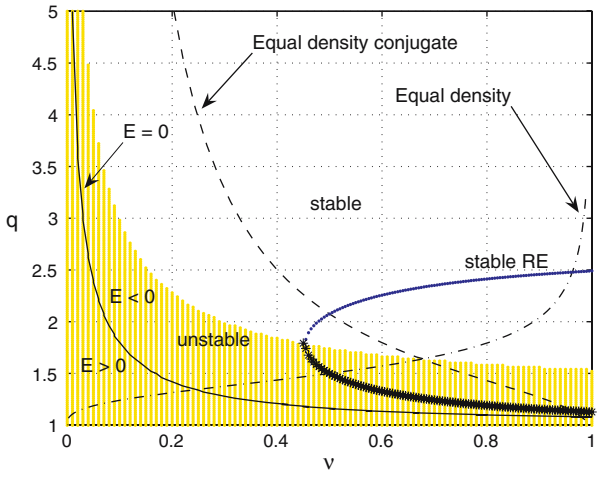

Fig. 6 Stability diagram for planar motion in the long-axis solution. The clear region denotes spectral stability while the shaded one denotes a single hyperbolic manifold instability. The U-shape represents a locus of solutions q as function of the mass ratio, for a constant angular momentum; we can find at most two solutions given a value of angular momentum. The upper and lower branches are stable and unstable solutions, respectively. The dashed and pointed dashed lines are equal density solutions with their conjugate. Ellipsoidal parameters are $\alpha = 1$, $\beta = 0.5$, $\gamma = 0.25$

relative equilibrium solution associated with a positive energy or not. For positive energy the equilibria are found to always be unstable. Furthermore, a positive total energy indicates that the system can disrupt under its mutual dynamics (Scheeres 2002). For negative energy the system is bound and the solutions can be stable or unstable. For a system dissipating energy, the free energy gives a measure of the energy that must be dissipated to transition from an unstable to a stable state.

Comparing Figs. 4, 5a, the U-shaped curve has its tip sitting on the stability transition of the relative equilibria solutions. The resulting plot is shown in Fig. 6. The lower branch is situated in the unstable shaded region of the plot while the upper branch is in the stable region. We also show how the U-shaped curve fits with the conjugate solutions; the dashed line on Fig. 6 are the conjugate solutions to the equal density solutions (pointed dashed line). The intersections of the U-shaped curve with the dashed line correspond to two solutions for equal density and the same angular momentum, having mass ratios of $\nu = 0.5$ and $\nu = 0.96$ in this case.

In addition to energy and stability properties, we can extract further information on the system evolution in terms of energy and momentum exchange. The U-shaped curve shifts to the right as the angular momentum is decreased which is shown in more detail on Fig. 7. Thus, for a system in relative equilibrium at a solution located on the lower branch of a given U-shaped curve, that is, in an unstable configuration, loosing angular momentum would make this solution move upwards. Hence the bodies become more distant when loosing angular momentum while approaching more stable configurations. Finally, a system with a higher value of angular momentum value may have a solution with its energy being positive. In this case, the system would first need to loose energy in order to become bound ($E < 0$) and then evolve towards a more stable configuration.

2.3 Notes on evolutionary scenarios for an ellipsoid–sphere system

The results on relative equilibria combined with analysis of the dynamics of particles in the vicinity of a binary system locked in its long-axis configuration (Bellerose and Scheeres 2006) provide insights on mass and momentum exchange that may occur between the two bodies. Bellerose and Scheeres (2006) we investigated the location of the analogue Lagrangian points and energy associated with a particle orbiting in this gravitational field. Since the mass

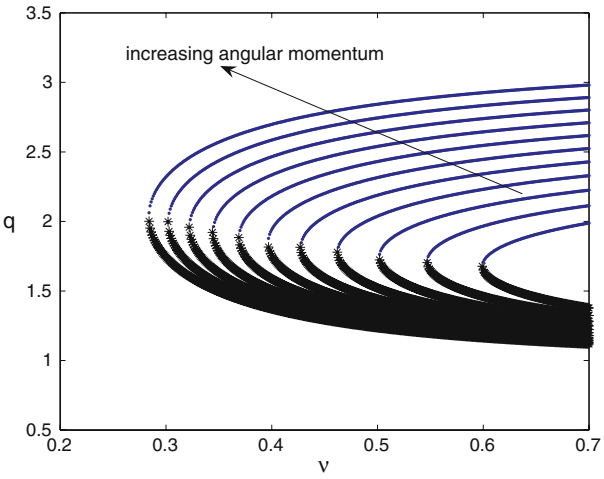

Fig. 7 Bifurcation solution q as function of the mass ratio ν, and values of angular momentum K, from 1.65 to 1.85 (nondimensional) $\gamma = \frac{1}{2}\beta = 0.5$. The lower and upper branches represent stable and unstable solutions, respectively

distribution of one of the bodies is now taken into account, L_1 is a key element for transfers between the bodies. It was shown that L_1 can be situated between or inside the bodies depending on the free parameters of the system modifying the transfer possibilities.

For the planar dynamics of a particle in this gravitational field, referred to as the Restricted Full Three-Body Problem, taken from Bellerose and Scheeres (2007b) the equilibrium solutions are computed from

$$\omega^2 x = \frac{\nu(x-(1-\nu)r)}{\left[(x-(1-\nu)r)^2+y^2+z^2\right]^{\frac{3}{2}}} + (1-\nu)(x+\nu r)R_{j\alpha}, \tag{34}$$

and

$$\omega^2 y = \frac{\nu y}{\left[(x-(1-\nu)r)^2+y^2+z^2\right]^{\frac{3}{2}}} + (1-\nu)yR_{j\beta}, \tag{35}$$

where ω is given by the solution of the F2BP, Eq. (19), and, in this case, x and y are the components of the position of the particle and r is the distance between the bodies in relative equilibrium.

The limiting case is for L_1 to sit on the ellipsoid facing the sphere. In this case, the location of the L_1 coordinate would be $(x_{L_1}, 0)$ where x_{L_1} is

$$x_{L_1} = 1 - \nu r. \tag{36}$$

Substituting x_{L_1} in Eq. (34), we obtain

$$\nu = \frac{\omega^2 - I(q)}{\left(\omega^2 r - \frac{1}{(r-1)^2} - I(q)\right)}. \tag{37}$$

Equation (37) is plotted on Fig. 8 showing the distance between the primaries r as a function of the mass ratio ν. The region above the solid line defines the parameters for which L_1 is outside of the ellipsoid; the region below the solid line represents cases of L_1 being inside the ellipsoid.

A reasonable assumption for binary systems is that they have the same density between the two bodies. To provide a better physical insight we compare the results of having L_1 sitting on the ellipsoid given above to the case of equal density between the two bodies. First,

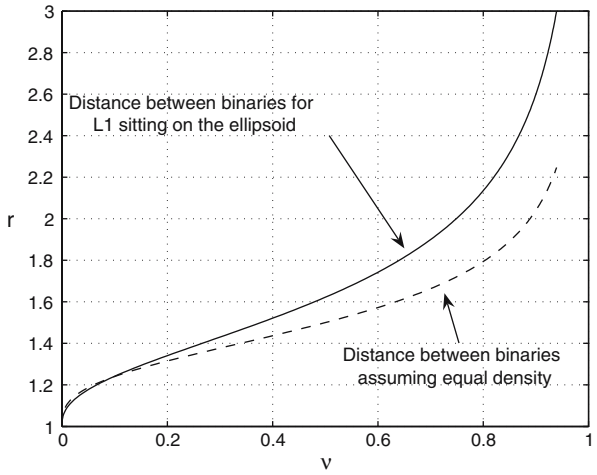

Fig. 8 Equations (37–41) are plotted together. The dash line represents the value of the two body distance for the case of constant density with the two bodies in contact. The solid line represents the locus of the mass ratio ν and the distance r between the bodies for L_1 to be sitting on the ellipsoid, facing the sphere. For an equal density binary, the transition for L_1 from inside to outside the ellipsoid happens at $r = 1.22$, $\nu = 0.08$. Ellipsoidal parameters are $[\alpha{:}\beta{:}\gamma] = [1{:}0.5{:}0.25]$

let's expand on an equal density binary system. From the definition of the mass ratio, ν, we have

$$\nu = \frac{M_1}{(M_1 + M_2)} = \frac{\frac{4\pi}{3}\rho R_s^3}{\frac{4\pi}{3}\rho(R_s^3 + \alpha\beta\gamma)}, \tag{38}$$

where R_s is the radius of the sphere. Solving for R_s, we obtain

$$R_s = \left[\alpha\beta\gamma\left(\frac{\nu}{1-\nu}\right)\right]^{\frac{1}{3}}. \tag{39}$$

Since the distance between the bodies can vary, and hence the location of L_1, the simplest situation is to have the two bodies stay in contact with each other. Then the distance between them can be varied. Here, with $\alpha = 1$ from our normalization, we denote the distance between the bodies as R and write

$$R = 1 + R_s. \tag{40}$$

Substituting R_s from Eq. (39) into Eq. (40), we can express the distance between the bodies as

$$R = 1 + \left[\beta\gamma\left(\frac{\nu}{1-\nu}\right)\right]^{\frac{1}{3}}. \tag{41}$$

Equation (41) is the dash line plotted on Fig. 8, the distance R as a function of the mass ratio ν.

From Eqs. (37–41), we can find conditions for L_1 to be inside or outside of a binary system with equal density. Given a value of the distance between the two bodies, r, we compute the required value of the mass ratio for L_1 touching the ellipsoid, from Eq. (37). Using this same mass ratio in Eq. (41), we then compute the corresponding distance R between two bodies with the same density. The meeting point on Fig. 8 indicates that L_1 is sitting on the ellipsoid for a case of equal density, which occurs for $r = 1.22$ and $\nu = 0.08$. Note that, in this simple case, the sphere is also touching the ellipsoid. As β increases, this transition limit is shifted up.

On Fig. 8, the region below the solid line indicates that $r < R$ meaning L_1 would be located inside the ellipsoid if the bodies were to be of equal density and resting on each other.

In the region above the solid line, $r > R$ and L_1 is in the exterior region of the ellipsoid. As the distance between the bodies increases, the path from the sphere to the ellipsoid would be open to particles leaving one of the body. The connecting region is found from computing the zero-velocity limits on the spherical body given a value for the Jacobi integral. Certain conditions would allow particles to transit from one body to the other, which are investigated in Bellerose and Scheeres (2006).

2.4 Stability analysis of relative equilibria in the F2BP

2.4.1 Spectral stability

Stability of relative equilibria is composed of two parts, spectral stability and energetic stability. The conditions for spectral stability of a relative equilibrium of the F2BP were derived in Scheeres (2003). In this case it is more convenient to write them in terms of the Hamiltonian form of the equations of motion.

Given Eqs. (22–25), a small perturbation to the nominal path is

$$\begin{bmatrix} \delta\dot{\boldsymbol{q}} \\ \delta\dot{\boldsymbol{p}} \end{bmatrix} = J H_{xx} \begin{bmatrix} \delta\boldsymbol{q} \\ \delta\boldsymbol{p} \end{bmatrix}, \tag{42}$$

where J has the form

$$J = \begin{bmatrix} 0 & I \\ -I & 0 \end{bmatrix} \tag{43}$$

and I is the identity matrix.

H_{xx} represents the second derivatives of the Hamiltonian defined by Eq. (20),

$$H_{xx} = \begin{bmatrix} -\sigma\omega^2 + U_{q_xq_x} & 0 & 0 & \omega(1-\sigma) \\ 0 & U_{q_yq_y} & -\omega & 0 \\ 0 & -\omega & -1 & 0 \\ \omega(1-\sigma) & 0 & 0 & -(1+\sigma) \end{bmatrix}. \tag{44}$$

In these expressions, $\sigma = \nu {q_x}^2 / I_{zz}$, and we used $\omega = \frac{(\nu K / I_{zz})}{(1+\sigma)} = \sqrt{I(q)}$ from substituting the relative equilibrium equation for p, Eq. (31), into the angular velocity equation, defined by Eq. (19). The second order derivatives $U_{q_xq_x}$ and $U_{q_yq_y}$ are given in the Appendix.

The characteristic equation of $J H_{xx}$ is found to be

$$\zeta^4 + a\zeta^2 + b = 0, \tag{45}$$

where

$$a = 2\omega^2(1-\sigma) + B - (1+\sigma)U_{q_yq_y}, \tag{46}$$

$$b = \omega^2(1-\sigma)^2(U_{q_yq_y} + \omega^2) - B(U_{q_yq_y} + \omega^2)(1+\sigma), \tag{47}$$

and $B = \sigma\omega^2 - U_{q_xq_x}$.

For stability to hold, the conditions to satisfy are

$$a > 0, \tag{48}$$

$$b > 0, \tag{49}$$

and

$$a^2 - 4b > 0. \tag{50}$$

In the case of a stable equilibrium solution, the system only has a center manifold and we can compute two sets of imaginary eigenvalues. For an eigenvalue of the type $\zeta = \pm i\lambda$, the period of oscillation is computed using

$$T = \frac{2\pi}{\lambda}. \tag{51}$$

Hence, each stable solution has two frequencies associated with it.

An unstable solution will have one pair of imaginary and one pair of real eigenvalues. The real eigenvalues are associated with a hyperbolic manifold which make the solution unstable. Note that it is still possible to obtain the associated frequency of oscillation for the system. Scheeres (2003) provides a more detailed derivation of these stability conditions. An example of stability regions was shown in Fig. 4.

As mentioned in the previous section, in general it is possible to find two solutions for given values of angular momentum, mass ratio and ellipsoidal parameters. There is always one stable and one unstable solution which also correspond to the energetic stability of the system discussed in the following section.

2.4.2 Energetic stability

Stability of a dynamical system can also be defined from its energy evaluation. A system is energetically stable if there is no state at the same angular momentum with a lower energy value. Scheeres (2006) energetic stability conditions are derived for a general gravity field in the F2BP under constant angular momentum assumption. This corresponds to nonlinear stability. In this section, we apply the method for our ellipsoid–sphere system model.

For stability of the equilibrium states, we need to investigate the second variation of the energy functional. We can write it in the form

$$d^2H = d\boldsymbol{x} \cdot H_{xx} \cdot d\boldsymbol{x} > 0, \tag{52}$$

where H_{xx} is given by Eq. (44) and the $d\boldsymbol{x}$ are chosen arbitrarily.

We find the energetic stability conditions from the eigenvalues of H_{xx}. The characteristic equation is found to be

$$\eta^4 + \alpha_3\eta^3 + \alpha_2\eta^2 + \alpha_1\eta + \alpha_0 = 0, \tag{53}$$

where the coefficients are expressed as

$$\alpha_3 = \left(U_{q_yq_y} - 2 - \sigma - B\right), \tag{54}$$

$$\alpha_2 = B\left(-U_{q_yq_y} + (2+\sigma)\right) + 1 + \sigma - U_{q_yq_y}(2+\sigma) - \omega^2 - \omega^2(1-\sigma)^2, \tag{55}$$

$$\begin{aligned}\alpha_1 = {} & B\left(U_{q_yq_y}(2+\sigma) + \omega^2 - (1+\sigma)\right) + \omega^2(-U_{q_yq_y} + 1)(1-\sigma)^2 \\ & + (U_{q_yq_y} + \omega^2)(1+\sigma),\end{aligned} \tag{56}$$

$$\alpha_0 = -B(U_{q_yq_y} + \omega^2)(1+\sigma) + \omega^2(U_{q_yq_y} + \omega^2)(1-\sigma)^2, \tag{57}$$

and $B = \sigma\omega^2 - U_{q_xq_x}$.

For a system to be stable, the real part of the eigenvalues all need to be positive. In this case, the energy is at a local minimum and the system cannot decrease its energy without decreasing its angular momentum. We can apply the Routh criteria to find analytical

conditions for energetic stability. The Routh criteria states that all roots of a polynomial of degree 4 have negative real parts if

$$\alpha_3 > 0, \tag{58}$$
$$\alpha_3\alpha_2 - \alpha_1 > 0, \tag{59}$$
$$\alpha_2\alpha_1 - \alpha_0\alpha_3 > 0, \tag{60}$$
$$\alpha_0 > 0. \tag{61}$$

Alternatively, we can also find the number of roots with positive real part by applying the Descartes' Law of Signs. This law states that the number of positive roots of a polynomial of degree n is equal to the number of sign changes in its coefficients, or is less than that number by a multiple of 2. In the present case, we would need

$$\alpha_3 < 0, \tag{62}$$
$$\alpha_2 > 0, \tag{63}$$
$$\alpha_1 < 0, \tag{64}$$
$$\alpha_0 > 0. \tag{65}$$

From investigating the conditions for spectral and energetic stability, we find a relation that links the two types of stability in the F2BP. By comparing Eq. (45) and Eq. (53) we note that the expression for b and α_0 are equivalent. Also, we find that spectral stability is lost as b transitions from $b > 0$ to $b < 0$. When the F2BP becomes spectrally unstable, $\alpha_0 < 0$ which makes one root of Eq. (53) to be in the left half plane. Hence, the system also becomes energetically unstable. Conversely, when the system is spectrally stable it is energetically stable.

In Fig. 5b we showed the corresponding energy of the relative equilibria under constant angular momentum, Fig. 5a. For a given mass ratio, the two solutions don't have the same stability properties; they are either spectrally and energetically stable or unstable. The lower branch of Fig. 5b corresponding to the upper branch of Fig. 5a are stable points. Hence, closer relative equilibria are unstable and associated with a larger energy than the more distant relative equilibria, which are stable. We can naturally suspect that a system dissipating energy could transition from a closer unstable configuration to a more distant stable one. Note that the stability of the bifurcation point is indeterminate.

2.5 Periodic orbits in the F2BP

Non-equilibrium dynamics of the F2BP are more commonly found in nature. In this case, the complete equations of motion defined by Eqs. (22–25) need to be solved. As a next step, we are interested in investigating regions near relative equilibria, especially symmetric periodic orbits. We can show that a small disturbance from the relative equilibria lead to periodic orbit with the minimum energy value of the periodic orbit family being the corresponding relative equilibria.

2.5.1 Poincaré map reduction method

Our computation of periodic orbits are performed using a Poincaré map reduction method as discussed in Wiggins (1998). For this work, a surface of section, denoted $S(\boldsymbol{q})$, is chosen to be normal to the flow in the vicinity of a given solution, which allows to find symmetric periodic orbits. A convenient surface is a coordinate axis, or $q_i = 0$ in the Cartesian space.

The Poincaré map is defined as the solution $\boldsymbol{q}(t)$ crosses the surface with the condition that $\boldsymbol{q}(t)|_{q_x=S} \cdot \nabla(S) > 0$. With this surface of section, it is possible to remove one dimension from consideration using $S(\boldsymbol{q}) = 0$. If the system has a conserved quantity, another dimension can be removed.

We define the full state as

$$\boldsymbol{x} = \begin{bmatrix} q_x \\ q_y \\ p_x \\ p_y \end{bmatrix}, \tag{66}$$

and C is a vector of parameters. If we write the first return of the Poincaré map as being

$$x_i^1 = Q(x_i, C), \tag{67}$$

where x_i is a variable of the full state, then the nth iterate is

$$x_i^n = Q^n(x_i, C). \tag{68}$$

A periodic orbit is defined as a point $\boldsymbol{x}^*$ such that

$$\boldsymbol{x}^* = Q(\boldsymbol{x}^*, C). \tag{69}$$

Since a given initial condition $\boldsymbol{x_0}$ would not necessary give a true periodic orbit, we need to compute the correction to the state such that

$$\boldsymbol{x_0} + \Delta x = Q(\boldsymbol{x_0} + \Delta \boldsymbol{x}, C) = Q(\boldsymbol{x_0}) + \left.\frac{\partial Q}{\partial \boldsymbol{x}}\right|_{\boldsymbol{x_0}} \Delta \boldsymbol{x} + \cdots \tag{70}$$

Then,

$$\Delta \boldsymbol{x} = [I - \Phi(T)]^{-1} \left(Q(\boldsymbol{x_0}) - \boldsymbol{x_0}\right), \tag{71}$$

where $\Phi(T) = \left.\frac{\partial Q}{\partial \boldsymbol{x}}\right|_{\boldsymbol{x_0}}$. The method converges if started close enough to the fixed point, $\boldsymbol{x}^*$, and if the matrix in Eq. (71) is nonsingular (Flannery et al. 1996).

This method is used with the Hamiltonian form of the equations of motion. The surface of section is chosen to be the q_x axis, i.e., $q_y = 0$. To extend the map to its first linear variation, we compute the four dimensional state transition matrix of the system, denoted as $\Phi_{i,j}$, where $i, j = 1, 2 \ldots 4$. Since in this time-invariant system, a closed trajectory has two unity eigenvalues, the state transition matrix is degenerate at the periodic orbit. Due to this, we must remove variations along the surface of section and the energy integral. In the following, we apply the method described in Scheeres et al. (2000).

With the surface of section and the energy integral, it is possible to remove two coordinate dimensions, q_y and p_y, leading to a two-dimensional monodromy matrix. In order to do so, we constrain the linear variation to lie on the Poincaré surface.

In the vicinity of a periodic orbit, the first return of q_y is not necessary zero. It is expressed as

$$\Delta q_y(T) = \sum_{\substack{j=1 \\ j \neq 2}}^{4} \Phi_{2j}(T, 0) \Delta x_j(0), \tag{72}$$

where $i, j = 1, 3$ or 4, and T is the return time. To force $\Delta q_y(T)$ to be zero, we introduce a small variation of return time ΔT such that

$$\Delta q_y(T + \Delta T) = \sum_{\substack{j=1 \\ j \neq 2}}^{4} \Phi_{2j}(T, 0)\Delta x_j(0) + \dot{q_y}\Delta T = 0. \tag{73}$$

In solving for ΔT, the linear variation of the Poincaré map becomes

$$\Psi_{i,j} = \Phi_{i,j}(T) - \frac{\dot{x_i}}{\dot{q_y}}\Phi_{2j}(T). \tag{74}$$

Now using the energy integral, we solve for the p_y coordinate which is transverse to the surface of section to remove one more dimension. This gives

$$\Delta p_y = -\frac{1}{E_{p_y}}(E_{q_x}\Delta q_x + E_{p_x}\Delta p_x), \tag{75}$$

where E is the energy integral given by Eq. (20). We apply this at the initial time, $t = 0$, and substitute for Δp_y to end up with the final form of the 2×2 monodromy matrix, $\Psi(T)$

$$\Psi_{i,j} = \Phi_{i,j}(T) - \frac{\dot{x_i}}{\dot{q_y}}\Phi_{2,j}(T) - \frac{1}{\dot{q_y}(0)}\left[\Phi_{i,4}(T) - \frac{\dot{x_i}}{\dot{q_y}}\Phi_{2,4}(T)\right]\frac{\partial E}{\partial x_j}(0), \tag{76}$$

where $i, j = 1, 3$.

Therefore, we solve the dynamical system until the condition $q_y = 0$ is met and we compute the monodromy matrix from the state transition matrix using Eq. (76). If we define the reduced state

$$\boldsymbol{y} = \begin{bmatrix} q_x \\ p_x \end{bmatrix} \tag{77}$$

in the vicinity of a periodic orbit, we can calculate the correction to the initial reduced state from

$$\Delta \boldsymbol{y} = (I - \Psi(T))^{-1}(Q(\boldsymbol{y_0}) - \boldsymbol{y_0}) \tag{78}$$

where $\Psi(T)$ is the 2×2 monodromy matrix, $Q(\boldsymbol{y_0})$ is the computed reduced state and $\boldsymbol{y_0}$ is the initial reduced state.

This procedure gives correction to q_x and p_x as we removed two degrees of freedom from the map reduction method and energy integral. Correction to p_y is computed from conservation of the energy integral evaluated after one period

$$\Delta p_y = -\frac{1}{H_{p_y}}(H_{q_x}\Delta q_x + H_{p_x}\Delta p_x) \tag{79}$$

or

$$\Delta p_y = -\frac{1}{\dot{q_y}}(-\dot{p_x}\Delta q_x + \dot{q_x}\Delta p_x). \tag{80}$$

The new initial state is then updated by $\boldsymbol{x_0} = \boldsymbol{x_0} + \Delta \boldsymbol{x}$, and the process is iterated until the difference between the computed state $Q(\boldsymbol{y_0})$ and the initial state $\boldsymbol{y_0}$ is comparable to numerical solver tolerances. In the following sections, for convenience we report numerical values that converge to within 1% after the first iteration. However, the simulations shown were carried to absolute tolerance of 1×10^{-8}.

2.5.2 Stability analysis of periodic orbits

The stability of periodic orbits is analyzed from investigating the eigenvalues of the monodromy matrix. In Hénon (1965) and Scheeres (1992) describe an analytical procedure to characterize critical points of periodic orbits and perioic orbit families in the R3BP and for motion close to rings, respectively. We apply the method for the current problem.

First, recall the general expression for the monodromy matrix in Eq. (76),

$$\Psi = \begin{bmatrix} \Psi_{11} & \Psi_{12} \\ \Psi_{21} & \Psi_{22} \end{bmatrix}. \tag{81}$$

The monodromy matrix is a linearization around the fixed point of the full (nonlinear) Poincaré map. Points on the surface of section are mapped according to

$$\begin{bmatrix} \Delta q_x \\ \Delta p_x \end{bmatrix} = \begin{bmatrix} \Psi_{11} & \Psi_{12} \\ \Psi_{21} & \Psi_{22} \end{bmatrix} \begin{bmatrix} \Delta q_{x0} \\ \Delta p_{x0} \end{bmatrix}. \tag{82}$$

Note that the entries of the monodromy matrix are evaluated at the initial conditions for a periodic orbit and its determinant is

$$\Psi_{11}\Psi_{22} - \Psi_{12}\Psi_{21} = 1. \tag{83}$$

Since we start with the initial conditions, $q_{y0} = 0$ and $p_{x0} = 0$, the symmetry of the periodic orbit in space and time implies that $q_x(t) = q_x(-t)$ and $p_x(t) = -p_x(-t)$. Hence, we can write,

$$\begin{bmatrix} \Delta q_{x0} \\ \Delta p_{x0} \end{bmatrix} = \begin{bmatrix} \Psi_{11} & -\Psi_{12} \\ \Psi_{21} & \Psi_{22} \end{bmatrix} \begin{bmatrix} \Delta q_x \\ \Delta p_x \end{bmatrix}. \tag{84}$$

Inverting Eq. (84)

$$\begin{bmatrix} \Delta q_x \\ \Delta p_x \end{bmatrix} = \begin{bmatrix} \Psi_{22} & \Psi_{12} \\ \Psi_{21} & \Psi_{11} \end{bmatrix} \begin{bmatrix} \Delta q_{x0} \\ \Delta p_{x0} \end{bmatrix}. \tag{85}$$

Comparing Eqs. (82–85), we need $\Psi_{11} = \Psi_{22}$, or

$$\begin{bmatrix} \Delta q_x \\ \Delta p_x \end{bmatrix} = \begin{bmatrix} \Psi_{11} & \Psi_{12} \\ \Psi_{21} & \Psi_{11} \end{bmatrix} \begin{bmatrix} \Delta q_{x0} \\ \Delta p_{x0} \end{bmatrix}. \tag{86}$$

Note that the determinant of the monodromy matrix is then written as,

$$\Psi_{11}^2 - \Psi_{12}\Psi_{21} = 1. \tag{87}$$

The stability of the periodic orbit is investigated using the eigenvalues of the monodromy matrix, computed from Eq. (86),

$$\lambda^2 - 2\Psi_{11}\lambda + 1 = 0. \tag{88}$$

For the system to be stable, the only condition is on the first entry of the monodromy matrix, Ψ_{11}, stated as

$$-1 \leq \Psi_{11} \leq 1. \tag{89}$$

Providing Eq. (89), λ will have unit magnitude or $|\lambda| = 1$, resulting in stable periodic orbits. We see a change in stability as Ψ_{11} goes through ± 1.

2.5.3 Continuation properties

It is possible to continue a periodic family with respect to one of the system parameters C. From our assumption that a periodic orbit is expressed as $\boldsymbol{y}^* = Q(\boldsymbol{y}^*, C)$, a nearby periodic orbit will satisfy

$$\boldsymbol{y}^* + \Delta\boldsymbol{y} = Q(\boldsymbol{y}^* + \Delta\boldsymbol{y}, C + \Delta C) \tag{90}$$

Expanding Eq. (90), we get

$$\boldsymbol{y_0} + \Delta\boldsymbol{y} = Q(\boldsymbol{y_0} + \Delta\boldsymbol{y}, C + \Delta C) = Q(\boldsymbol{y_0}, C) + \left.\frac{\partial Q}{\partial \boldsymbol{y}}\right|_{\boldsymbol{y_0}} \Delta\boldsymbol{y} + \left.\frac{\partial Q}{\partial C}\right|_{\boldsymbol{y_0}} \Delta C \cdots \tag{91}$$

Let's use the definition for the monodromy matrix as given by Eq.(81) and the following expression for $\left.\frac{\partial Q}{\partial C}\right|_{\boldsymbol{y_0}}$,

$$\frac{\partial Q}{\partial C} = [h_1, h_2]^T. \tag{92}$$

Using Eqs. (81–92) into Eq. (91), we can express $\Delta\boldsymbol{y}$ in the following form,

$$\begin{bmatrix} \Delta q_x \\ \Delta p_x \end{bmatrix} = \begin{bmatrix} \Psi_{11} & \Psi_{12} & h_1 \\ \Psi_{21} & \Psi_{11} & h_2 \end{bmatrix} \begin{bmatrix} \Delta q_x \\ \Delta p_x \\ \Delta C \end{bmatrix}. \tag{93}$$

From the symmetry property in space and time, a variation in p_x will have no effect on q_x or the system parameter C, as $p_{x_0} = 0$. Hence, this allows us to decouple the system and re-write Eq. (93) as

$$\begin{bmatrix} 0 \\ 0 \end{bmatrix} = \begin{bmatrix} \Psi_{11} - 1 & h_1 \\ \Psi_{21} & h_2 \end{bmatrix} \begin{bmatrix} \Delta q_x \\ \Delta C \end{bmatrix} \tag{94}$$

and

$$\begin{bmatrix} 0 & 0 \end{bmatrix} = \begin{bmatrix} \Psi_{12} & \Psi_{11} - 1 \end{bmatrix} \Delta p_x. \tag{95}$$

For the system to have a non-trivial solution, from Eq. (94), we need

$$\begin{vmatrix} \Psi_{11} - 1 & h_1 \\ \Psi_{21} & h_2 \end{vmatrix} = 0, \tag{96}$$

giving

$$(\Psi_{11} - 1)h_2 - h_1\Psi_{21} = 0. \tag{97}$$

In investigating for possible singular values in Eqs. (87–97), three cases need to be considered, $\Psi_{11} = 1$, $\Psi_{11} = -1$ and $\Psi_{11} \neq 1$.

2.5.4 Case of $\Psi_{11} = 1$

In the case $\Psi_{11} = 1$, Eqs. (87–97) become,

$$\Psi_{12}\Psi_{21} = 0 \tag{98}$$

and

$$h_1\Psi_{21} = 0. \tag{99}$$

At this value a stability transition can occur. First, if $\Psi_{21} \neq 0$ and $\Psi_{12} = 0$, we find an explicit relation between Δq_x and ΔC,

$$\Delta q_x = -\frac{h_2}{\Psi_{21}} \Delta C. \tag{100}$$

In addition, $h_1 = 0$ in order to satisfy Eq. (94). Then, from Eq. (95), we find that Δp_x is arbitrary implying an intersection with a non-symmetric periodic orbit of the same period (Wiggins 1998).

On the other hand, if $\Psi_{21} = 0$ and $\Psi_{12} \neq 0$, Eqs. (94) become

$$h_1 \Delta C = 0 \tag{101}$$

and

$$h_2 \Delta C = 0. \tag{102}$$

Also, from Eq. (95), we have now

$$\Psi_{12} \Delta p_x = 0. \tag{103}$$

From these equations above, we have that $\Delta p_x = 0$ implying that intersection with a non-symmetric family does not occur.

If $h_1 = h_2 = 0$, Δq_x and ΔC are arbitrary, not unique and free to vary indicating an intersection with another symmetric family of the same period. On the other hand, if h_1 or h_2 are not null, we have $\Delta C = 0$. In this case there is no intersection with another family and the periodic orbit family is at a local extremum of the system parameter C (Wiggins 1998).

2.5.5 *Case of* $\Psi_{11} = -1$

Now consider the case of $\Psi_{11} = -1$. Again, a stability transition can occur. Equations (87–97) become

$$\Psi_{12} \Psi_{21} = 0, \tag{104}$$

which we had before, and

$$h_1 \Psi_{21} = 2h_2. \tag{105}$$

We can again consider both situations where $\Psi_{12} = 0$ and $\Psi_{21} = 0$. If $\Psi_{12} = 0$, Eqs. (94, 95) become

$$-2\Delta q_x + h_1 \Delta C = 0 \tag{106}$$

and

$$\Psi_{21} \Delta q_x + h_2 \Delta C = 0, \tag{107}$$

with

$$\Delta p_x = 0 \tag{108}$$

and

$$-2\Delta p_x = 0. \tag{109}$$

This implies an intersection with a symmetric family of twice the period (Wiggins 1998). In this case there is no condition on h_1 and h_2. A similar result is obtained when considering $\Psi_{21} = 0$. However, we need $h_2 = 0$ to satisfy Eq. (105). From Eqs. (94, 95), we have

$$\Delta q_x = \frac{h_1}{2} \Delta C. \tag{110}$$

Note that, in these cases, we can look at the nature of the double period family itself which should be consistent with the current monodromy matrix analysis. If Ψ is the monodromy matrix for the single period family, then at the intersection point, the monodromy matrix of the double period family should have the form Ψ^2. Hence, this should correspond to cases described in Sect. 2.5.4 where the double period family would most likely be at an extremum in one of its parameters.

2.5.6 *Case of* $\Psi_{11} \neq 1$

Finally, let's consider the case of $\Psi_{11} \neq 1$. In this case we consider the general equations given by Eqs. (87, 94, 97). Since both of the Δp_x coefficients are non zero, $\Delta p_x = 0$ which indicate there is no intersection with a non-symmetric family.

Equation (94) define the tangent curves to the family

$$\Delta q_x = -\frac{h_1}{\Psi_{11} - 1}\Delta C \tag{111}$$

and

$$\Delta q_x = -\frac{h_2}{\Psi_{21}}\Delta C. \tag{112}$$

The case $h_1 = 0$ or $h_2 = 0$ implies $h_2 = 0$ or $h_1 = 0$, respectively. This leads to having a local extremum with respect to q_x. Otherwise there is a one-to-one relationship between the periodic family and parameter C. In general, we can find two solutions for Δq_x as shown in Fig. 6.

Table 1 summarizes the cases mentioned. We can see that no cases lead to intersections with asymmetric periodic orbits, and so we do not extend the methods to asymmetric periodic orbits.

Table 1 Summary of stability conditions for a periodic orbit

Cases	Ψ_{11}	Ψ_{12}	Ψ_{21}	h_1	h_2	Δq_x	Δp_x	ΔC	Remarks
a	1	0	$\neq 0$	0	$\neq 0$	$-\frac{h_2}{\Psi_{21}}\Delta C$	$\neq 0$	$\neq 0$	Intersection with an asymmetric periodic orbit family of the same period
b	1	$\neq 0$	0	$\neq 0$	$\neq 0$	$\neq 0$	0	0	No intersection with symmetric families, the periodic orbit family is at a local extremum of C
c	1	$\neq 0$	0	0	0	$\neq 0$	0	$\neq 0$	Intersection with another symmetric family of the same period
d	-1	0	$\neq 0$	$\neq 0$	$\neq 0$	$\neq 0$	0	$\neq 0$	Intersection with a symmetric family of twice the period
e	-1	$\neq 0$	0	$\neq 0$	0	$\frac{h_1}{2}\Delta C$	$\neq 0$	$\neq 0$	Intersection with an asymmetric family of twice the period
f	$\neq 1$	$\neq 0$	$\neq 0$	$\neq 0$	$\neq 0$	2 RE	0	$\neq 0$	No intersection
g	$\neq 1$	$\neq 0$	$\neq 0$	0	0	0	0	$\neq 0$	No intersection, local extremum in q_x

Ψs are the components of the monodromy matrix while hs are derivatives with respect to a free parameter of the system, like the energy, denoted C. q_x and p_x are x-component of the position and inertial velocity. The notation "2 RE" indicates two relative equilibrium solutions

2.5.7 Continuation with respect to the energy and the period

We now apply these results to continuation with respect to the system energy and period. Equation (91) can be re-written to express the new correction term, $\Delta \boldsymbol{y_C}$, as a function of ΔC,

$$\Delta \boldsymbol{y_C} = [I - \Psi(T)]^{-1} \left. \frac{\partial Q}{\partial C} \right|_{y^*} \Delta C. \tag{113}$$

In the current problem, the method was applied for variation of the energy, E, and for the period, T. In the case of energy, the new correction term, $\Delta \boldsymbol{y_E}$, is found by,

$$\Delta \boldsymbol{y_E} = [I - \Psi(T)]^{-1} \left. \frac{\partial \boldsymbol{y}}{\partial E} \right|_{y^*} \Delta E. \tag{114}$$

The expression for $\frac{\partial \boldsymbol{y}}{\partial E}$ is given by,

$$\frac{\partial y_i}{\partial E} = \left[\Phi_{ie} - \frac{\Phi_{pe} \dot{y_i}}{\dot{q_y}} \right] \frac{1}{\frac{\partial E}{\partial p_y}}, \tag{115}$$

where i is either 1 ($y_1 = q_x$) or 3 ($y_3 = p_x$), p is the index of the Poincaré map reduction (2, for q_y), and e is the index of the removed variable (4, for p_y).

Since the period is related to the energy, continuation with respect to the period has a slightly different form to account for this,

$$\Delta \boldsymbol{y_T} = [I - \Psi(T)]^{-1} \left(+ \left. \frac{\partial \boldsymbol{y}}{\partial T} \right|_{y^*} \Delta T + \left. \frac{\partial \boldsymbol{y}}{\partial E} \right|_{y^*} \Delta E \right). \tag{116}$$

From our Poincaré map definition, we have

$$q_y(T + \Delta T) = 0 = q_y(T) + \dot{q}_y \Delta T + \frac{\partial q_y}{\partial E} \Delta E. \tag{117}$$

Or,

$$\dot{q}_y \Delta T = -\frac{\partial q_y}{\partial p_y} \frac{\partial p_y}{\partial E} \Delta E. \tag{118}$$

For a variation in the state $\boldsymbol{y}$, we also have that,

$$\Delta \boldsymbol{y} = \dot{y}_i \Delta T + \frac{\partial y_i}{\partial p_y} \frac{\partial p_y}{\partial E} \Delta E, \tag{119}$$

where i takes value for q_x and p_x, i.e., $i = 1, 3$. Hence, for a continuation using the period, substituting Eq. (118) into Eq. (119), we arrive at the following final expression for the correction term $\Delta \boldsymbol{y_T}$,

$$\Delta \boldsymbol{y_T} = [I - \Psi(T)]^{-1} \left(\dot{y}_i - \dot{q_y} \frac{\partial y_i}{\partial p_y} \frac{\partial p_y}{\partial q_y} \right) \Bigg|_{y^*} \Delta T. \tag{120}$$

The corrected initial state is then fed into the Poincaré map method to converge to a periodic orbit again. Note that for cases of singularity with respect to the energy and the period, we terminate the periodic orbit families by doing a linear analysis, such as in Sect. 2.5.4.

2.5.8 Near relative equilibria approximation

To simplify the analysis, we also derive an approximation method to model the dynamics in the F2BP near relative equilibria. We use the method of perturbations using eigenvalues and eigenvectors to generate the appropriate dynamics and solve for periodic orbits.

Using the eigenvalues and eigenvectors of the system given by Eqs. (42–44), a solution is given by

$$\begin{bmatrix} \boldsymbol{\delta q} \\ \boldsymbol{\delta p} \end{bmatrix} = e^{\lambda_a t} \begin{bmatrix} \boldsymbol{u} \\ \boldsymbol{v} \end{bmatrix}, \tag{121}$$

where λ_a is an eigenvalue and $\boldsymbol{u}$ and $\boldsymbol{v}$ are the corresponding eigenvectors.

For stable motion, $\lambda_a = \pm i\omega_a$. And the general orbit is described by the corresponding set of eigenvectors, $\boldsymbol{u} = \boldsymbol{\alpha} \pm i\boldsymbol{\beta}$. Therefore, the periodic perturbation can be written as

$$\begin{bmatrix} \boldsymbol{\delta q} \\ \boldsymbol{\delta p} \end{bmatrix} = \frac{1}{2}(a\boldsymbol{\alpha} - b\boldsymbol{\beta})\left[e^{i\omega_a t} + e^{-i\omega_a t}\right] - \frac{1}{2}(b\boldsymbol{\alpha} + a\boldsymbol{\beta})\left[e^{i\omega_a t} - e^{-i\omega_a t}\right]. \tag{122}$$

Note that the constants $(a \pm ib)$ satisfy the condition for a real solution.

Using trigonometric identities, we write Eq. (122) as

$$\begin{bmatrix} \boldsymbol{\delta q} \\ \boldsymbol{\delta p} \end{bmatrix} = (a\boldsymbol{\alpha} - b\boldsymbol{\beta})\cos(\omega_a t) - (b\boldsymbol{\alpha} + a\boldsymbol{\beta})\sin(\omega_a t) \tag{123}$$

In order to solve for the constant and initial conditions, first assume

$$\begin{bmatrix} \delta q_{x0} \\ \delta q_{y0} \end{bmatrix} = \begin{bmatrix} a\alpha_{qx} - b\beta_{qx} \\ a\alpha_{qy} - b\beta_{qy} \end{bmatrix} = \begin{bmatrix} \delta q_0 \\ 0 \end{bmatrix}. \tag{124}$$

Then, solving for a and b,

$$\begin{bmatrix} a \\ b \end{bmatrix} = \frac{1}{\alpha_{qy}\beta_{qx} - \alpha_{qx}\beta_{qy}} \begin{bmatrix} -\beta_{qy}\delta q_0 \\ -\alpha_{qy}\delta q_0 \end{bmatrix}, \tag{125}$$

we solve for initial conditions on $\boldsymbol{\delta p}$,

$$\begin{bmatrix} \delta p_{x0} \\ \delta p_{y0} \end{bmatrix} = \frac{\delta q_0}{\alpha_{qy}\beta_{qx} - \alpha_{qx}\beta_{qy}} \begin{bmatrix} 0 \\ \alpha_{qy}\beta_{py} - \alpha_{py}\beta_{qy} \end{bmatrix}. \tag{126}$$

Hence, to first order approximation, a periodic orbit near a relative equilibrium is described by

$$\begin{bmatrix} \boldsymbol{q_{RE}} + \boldsymbol{\delta q} \\ \boldsymbol{p_{RE}} + \boldsymbol{\delta p} \end{bmatrix}, \tag{127}$$

where $\boldsymbol{q_{RE}}$ and $\boldsymbol{p_{RE}}$ are values at relative equilibrium, $\boldsymbol{\delta q}$, $\boldsymbol{\delta p}$, a and b are given by Eq. (123) and Eq. (125) respectively. The initial conditions are written as follows,

$$\begin{bmatrix} q_{x0} \\ q_{y0} \\ p_{x0} \\ p_{y0} \end{bmatrix} = \begin{bmatrix} q_{xRE} + \delta q_0 \\ 0 \\ 0 \\ p_{yRE} + \left(\frac{\alpha_{qy}\beta_{py} - \alpha_{py}\beta_{qy}}{\alpha_{qy}\beta_{qx} - \alpha_{qx}\beta_{qy}}\right)\delta q_0 \end{bmatrix}. \tag{128}$$

The method of eigenvalues gives a good approximation to the results obtained using the Poincaré map method in the vicinity of the relative equilibria. It is important to note that the two methods developed to find periodic orbits in the F2BP can complement each other. The computations and initial guesses to converge to a periodic orbit using the Poincaré map

can be tedious. By using the approximation method to generate the initial conditions, one can then use these values as initial guesses to start the Poincaré map method. The procedure is very useful to compute periodic orbits close to each other but from different families and to converge on unstable periodic orbits.

2.6 Periodic orbits near relative equilibria for an ellipsoid–sphere system

Applying the method described in the previous sections, we investigate a family of periodic orbits in the neighborhood of a given relative equilibrium. As a simple assumption we assume the bodies have equal density and we investigate the system parameter space with this particular constraint. The second solution found for this same angular momentum defines the "conjugate" relative equilibrium. As shown in Fig. 9, cases of mass ratio, $\nu = 0.15$, $\nu = 0.5$, and $\nu = 0.85$, were studied.

We first concentrate on an equal mass ratio, $\nu = 0.5$, with equal density of the bodies. Using Eq. (19), we compute the spin rate, ω, and the corresponding value of the angular momentum, K. Then we solve for all solutions of the distance, q_x, between the bodies from Eq. (32). For this specific case, there exists two relative equilibrium at $q_x = 1.500$ and $q_x = 2.075$, which are the unstable and stable solutions, respectively (also shown on Fig. 6). Note that at $q_x = 1.500$ the two bodies are sitting on each other.

For this specific value of the angular momentum, at $q_x = 1.500$ we can compute one pair of imaginary eigenvalues and two sets of stable eigenvalues for $q_x = 2.075$. This allows us to find one family of periodic orbit for the unstable point and two for the stable one. The absolute minimum energy state, at $q_x = 2.075$, is the stable relative equilibrium point itself. Figure 10a, b show the evolution of one of the periodic orbits as they get closer to the equilibrium point; these periodic orbits usually enclose the equilibrium point and shrink in size as the energy is decreased. At the limit, the periodic orbit becomes a single point where the period of the periodic orbit matches the period of oscillation of the relative equilibrium. For the unstable family, for the unstable equilibrium, the period is $T_{URE} = 6.852$. For the stable equilibrium, we find the period to be $T_{SRE} = 13.558$ or 38.336 in normalized time units.

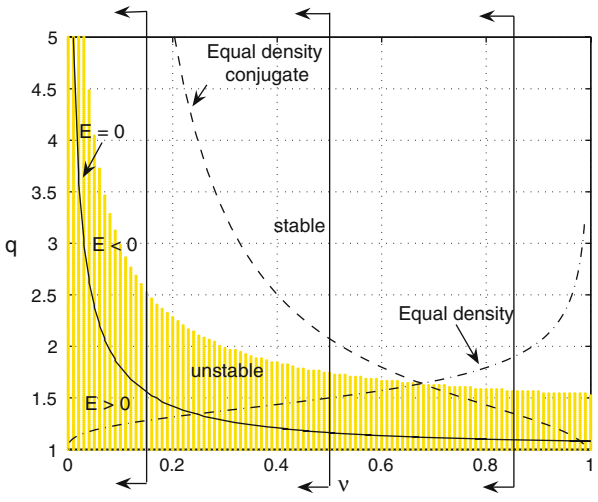

Fig. 9 Stability diagram for planar motion in the long-axis solution. We investigate families of periodic orbits and the general dynamics near $\nu = 0.15$, $\nu = 0.5$ and $\nu = 0.85$. Ellipsoid parameters are $\alpha = 1$, $\beta = 0.5$, and $\gamma = 0.25$

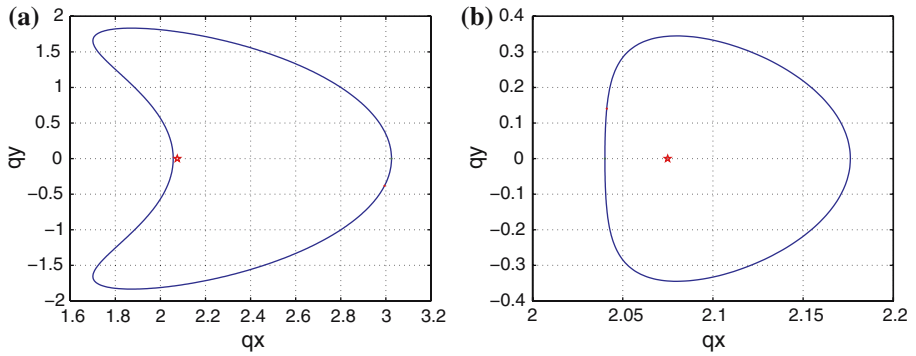

Fig. 10 Periodic orbit families for $\nu = 0.5$, $K = 1.715$ and ellipsoid parameters, $\alpha = 1$, $\beta = 0.5$ and $\gamma = 0.25$. Evolution of periodic orbits in a q_x–q_y coordinate frame near the $q_x = 2.075$ relative equilibrium having a period $T_{SRE} = 13.558$. (**a**) Periodic orbit: $q_{x0} = 3.021$ and $p_{y0} = 0.507$ with $E = -0.176$. (**b**) Periodic orbit: $q_{x0} = 2.182$ and $p_{y0} = 0.698$ with $E = -0.195$. The energy of the equilibrium solution, indicated by the starred point, is $E = -0.197$

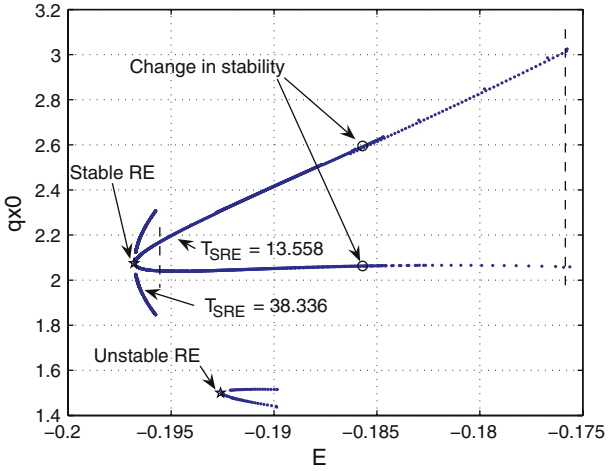

Fig. 11 Periodic orbit families for $\nu = 0.5$, $K = 1.715$ and ellipsoid parameters, $\alpha = 1$, $\beta = 0.5$ and $\gamma = 0.25$. Continuation for all three families of periodic orbits: q_{x0} vs. E. The two vertical dashed lines indicate the location of the two periodic orbits shown in Fig. 10

From using the continuation method, Fig. 11 shows the unstable family near $q_x = 1.500$ and the two families of periodic orbits, converging to $q_x = 2.075$. Note that these families have the same particular value of angular momentum but different energy. On this plot, the distance between the primary, q_{x0} is plotted as a function of the energy of the system, E. The star point represents the relative equilibrium or minimum energy point for this value of angular momentum. From this point, the upper and lower branches of each family are the two values of q_{x0} at which orbits of the family cross the q_y axis.

On Fig. 11, we also note a change in stability at the "o" point. In the region closer to the equilibrium point, the periodic orbits are stable. Otherwise, they are unstable. This critical point is found from investigating the eigenvalues of the monodromy matrix but can also be analyzed from entries of the monodromy matrix itself as described in the section on stability

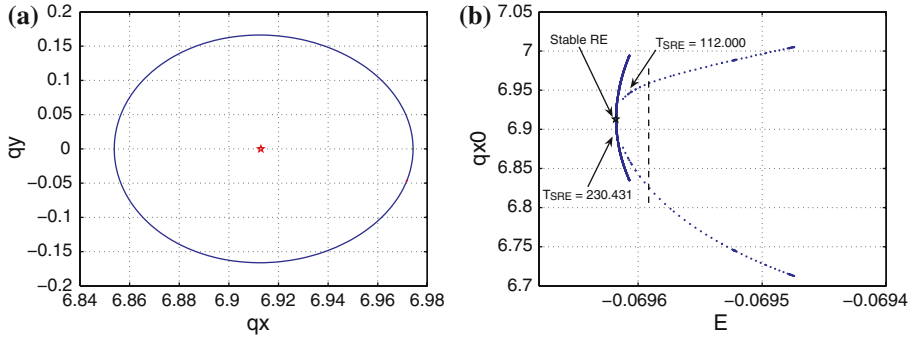

Fig. 12 (**a**) Periodic orbit: $q_{x0} = 6.974$ and $p_{y0} = 0.379$ with $E = -0.070$. (**b**) Periodic orbit families for $\nu = 0.15$, shown as q_{x0} vs. E. Note that the unstable family exists but is not shown. In (**a**) and (**b**), the ellipsoidal parameters are $[\alpha{:}\beta{:}\gamma] = [1{:}0.5{:}0.25]$. The vertical dashed line indicates the location of the periodic orbit shown in (**a**). The starred point is the stable relative equilibrium state, which has $E = -0.0696$

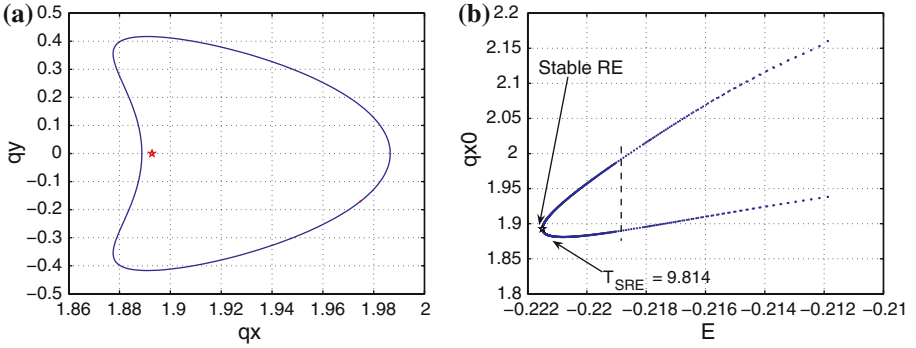

Fig. 13 (**a**) Periodic orbit: $q_{x0} = 1.985$ and $p_{y0} = 0.795$ with $E = -0.219$. (**b**) Periodic orbit families for $\nu = 0.85$, shown as q_{x0} vs. E. In (**a**) and (**b**), the ellipsoida parameters are $[\alpha{:}\beta{:}\gamma] = [1{:}0.5{:}0.25]$. The vertical dashed line indicates the location of the periodic orbit shown in (**a**). The starred point is the stable relative equilibrium state, which has $E = -0.222$

and continuation properties and shown on Table 1. In the present case, the critical point on Fig. 11 for which the stability changes has energy $E = -0.186$. This point intersects with a space-symmetric family of twice the period and we retrieve conditions as specified by case *e* on Table 1.

The previous analysis was obtained for an equally divided binary system. Having a dominant ellipsoid or a dominant sphere also affects these periodic orbit families. On Figs. 12, 13 we plotted periodic orbits and family continuations for cases of equal density binary systems with mass ratios of 0.15 and 0.85, respectively, in the vicinity of the stable relative equilibrium (see Fig. 9). For $\nu = 0.15$, stable and unstable equilibria are $q_x = 6.913$ and $q_x = 1.285$, respectively, where the periods of the stable equilibrium are $T_{SRE} = 230.431$ and 112.000, labeled in Fig. 12b. Note that only the shorter period family is shown for $\nu = 0.85$ in Fig. 13b, where $T_{SRE} = 9.814$ for its stable equilibrium at $q_x = 1.893$. This stable equilibrium has a long period $T_{SRE} = 27.988$. We see that the periodic orbits are reduced in size for small mass ratio; for similar wideness on the q_x axis, the orbits become taller as the mass ratio increases. Periodic orbits can also have the relative equilibrium solution outside of the orbit for large mass ratio.

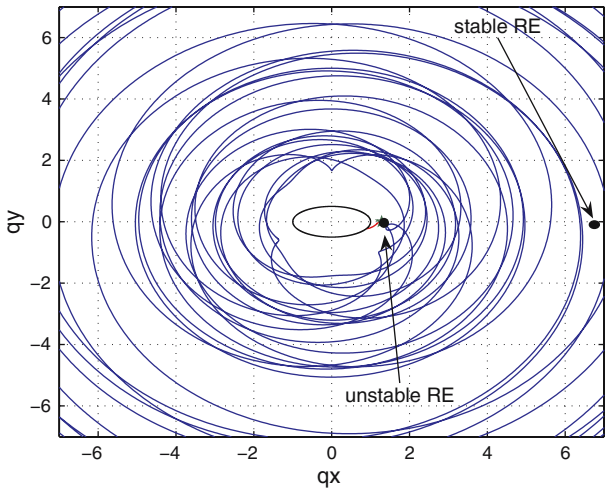

Fig. 14 Dynamics in the F2BP when the bodies are close to being at the closer unstable relative equilibrium. The trajectories following the unstable manifold cross the stable trajectories. Under energy dissipation, transition from an unstable to a stable state may be possible. The system mass ratio is $\nu = 0.15$ with a "free energy" $\Delta E = 0.335$. Ellipsoidal parameters are $[\alpha{:}\beta{:}\gamma] = [1{:}0.5{:}0.25]$

We also note that periodic orbits can be found in the vicinity of the bifurcation point where stable and unstable relative equilibria meet (see Fig. 6) for all values of the mass ratios. Looking at the 2×2 monodromy matrix, we can link these points to the minimum energy case in Table 1, i.e., case b. Finally, we retrieve case c for $\nu = 0.68$ and $q_x = 1.641$, associated with an energy $E = -0.223$, which corresponds to the meeting point of the equal density solution and its conjugate solution.

Current theories of binary systems formation included ones where a system may have dissociated from a single body (Scheeres 2007). If we keep in mind that a closer equilibrium configuration is unstable and the system may dissipate energy, it is natural to investigate possible transition of the system to reach a more stable orbit. Figures 14–16 show simulations for mass ratios of $\nu = 0.15$, $\nu = 0.25$ and $\nu = 0.5$ when the equal density binary system starts near an unstable relative equilibrium, with the bodies sitting on each other. In Fig. 14, since the system starts with a positive energy, that is $E = 0.265$, the bodies may escape from each other. However, we see that the trajectories following the unstable manifold may cross the stable trajectories. Under energy dissipation, the system may eventually reach stable periodic orbits or even arrive at a stable equilibrium configuration at the minimum energy state, $E = -0.070$. Figure 15 shows the same simulation for $\nu = 0.25$. In this case, the system starts at the unstable configuration with a negative energy, $E = -0.016$. We see that the orbit is bounded and the bodies do not escape. Reaching $E = -0.119$ from energy dissipation, the system could achieve a stable configuration. The case of $\nu = 0.5$ is described in Fig. 16 where the two equilibria are much closer to each other, starting with $E = -0.192$, and with a stable configuration at $E = -0.196$.

This possible transition between an unstable and a stable configuration can be quantified from values of energy at the two relative equilibria, defined earlier by the "free energy" of the system ΔE in Eq. (33). For the dynamics in Fig. 14, the system has $\Delta E = 0.335$ starting near the unstable point with a positive energy. It needs to dissipate 80% of its free energy before getting bound, with $E = 0$. For $\nu = 0.25$, the system is already bound and has a free

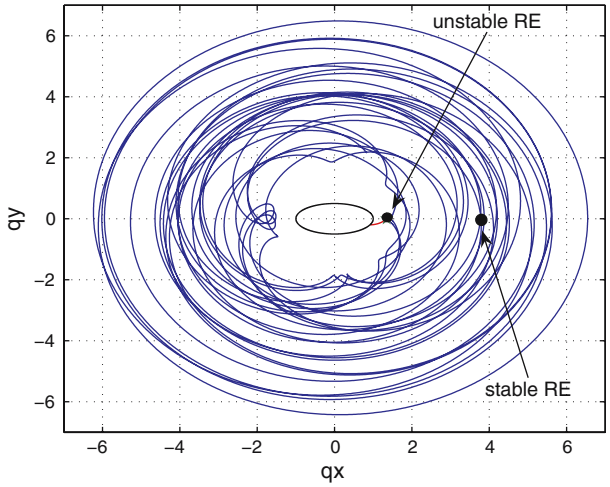

Fig. 15 Dynamics in the F2BP when the bodies are close to being at the closer unstable relative equilibrium. The trajectories following the unstable manifold cross the stable trajectories. Under energy dissipation, transition from an unstable to a stable state may be possible. The system mass ratio is $\nu = 0.25$ with a "free energy" $\Delta E = 0.135$. Ellipsoidal parameters are $[\alpha{:}\beta{:}\gamma] = [1{:}0.5{:}0.25]$

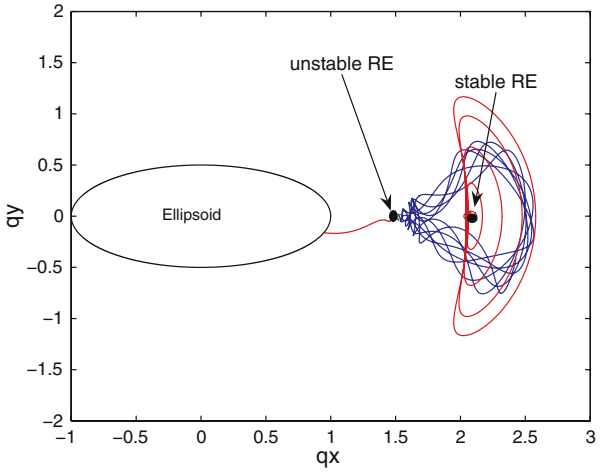

Fig. 16 Dynamics in the F2BP when the bodies are close to being at the closer unstable relative equilibrium. The trajectories following the unstable manifold cross the stable trajectories. Under energy dissipation, transition from an unstable to a stable state may be possible. The system mass ratio is $\nu = 0.5$ with a "free energy" $\Delta E = 0.004$. Ellipsoidal parameters are $[\alpha{:}\beta{:}\gamma] = [1{:}0.5{:}0.25]$

energy of $\Delta E = 0.135$. In Fig. 16, with a mass ratio of $\nu = 0.5$, the system's free energy is low, $\Delta E = 0.004$, making the trajectories near the unstable point stay close to the stable orbits. At $\nu = 0.85$, in this case there is no "free energy" at the unstable resting equilibrium point since this point lies inside the ellipsoid. Hence, at $q_x = 1.893$, the system is already at its lowest energetic point.

3 Conclusion

We provide a general description of the dynamics near relative equilibria in the Full Two Body Problem. We also compute and analyze the relative equilibria solutions and their stability for ellipsoidal parameters $\alpha = 1$, $\beta = 0.5$, and $\gamma = 0.25$. For a given value of angular

momentum, we show that there are in general two relative equilibrium solutions which are opposite in stability. Throughout its evolution, a binary system may go through different configurations and stability which can affect mass and angular momentum transfers between the bodies. We find that equilibrium configurations where the bodies are closer to each other are unstable and contain more energy than the "far" solutions, which are always stable with the minimum energy of the system. Under energy dissipation, the system may transition from one state to the other, especially if it is to gain stability.

Given small perturbations, we can link these equilibria to periodic orbits associated with the same value of angular momentum. The periodic orbits are computed using a Poincaré map reduction method on a two degree of freedom Hamiltonian system. Their stability is investigated from the eigenvalues of the monodromy matrix. In the vicinity of a relative equilibria, we also develop an approximate method to generate these periodic orbits using the stable eigenvalues and corresponding eigenvectors. We can find two stable families in the vicinity of a stable relative equilibrium and one unstable family associated to the unstable relative equilibrium. The minimum energy point of these periodic orbits match the relative equilibrium conditions where the absolute minimum state is always at the stable equilibrium configuration.

Finally, we look at the dynamics in the vicinity of these equilibria. Under certain conditions, a single body may split where the resulting dynamics of the bodies could follow the possible transitional paths, from unstable to stable states, described in this work. A system losing total energy from an unstable equilibrium configuration has the possibility of evolving towards a stable one. The dynamics of particles in this gravitational field, what we call the Restricted Full Three-Body Problem (RF3BP), is affected by the dynamics of the binary bodies. More analysis needs to be done in order to understand this dynamical coupling. In the near future, we plan to investigate the dynamics of the RF3BP under the effect of a periodic model for the F2BP. The stability properties of the equilibrium conditions in both the RF3BP and the F2BP may have different effects on the dynamics of the RF3BP.

Acknowledgements This research was funded, in part, by a grant from the Jet Propulsion Laboratory/ California Institute of Technology Director's Research and Development Fund. Julie Bellerose acknowledges support via a Fellowship from the Natural Sciences and Engineering Research Council of Canada.

Appendix: Mutual potential expressions

The first and second order partial derivatives of the mutual potential were given in Scheeres (2003). For convenience, they are rewritten here. For the first derivatives,

$$U_{q_x} = -\frac{3}{2} q_x \int_\lambda^\infty \frac{du}{(u+1)\Delta(u)}, \tag{129}$$

and

$$U_{q_y} = -\frac{3}{2} q_y \int_\lambda^\infty \frac{du}{(u+\beta^2)\Delta(u)}. \tag{130}$$

These derivatives are written in terms of the R_j expressions that are the elliptic integrals representing the mass distribution of the ellipsoid. Using the substitution $v = u + \lambda$, they can be solved as written in the following form and can be computed using algorithms from Flannery et al. (1996),

$$R_{j\alpha} = \frac{3}{2} \int_0^\infty \frac{du}{(u+\lambda+1)\Delta(u+\lambda)}, \tag{131}$$

$$R_{j\beta} = \frac{3}{2}\int_0^\infty \frac{du}{(u+\lambda+\beta^2)\Delta(u+\lambda)}, \tag{132}$$

and

$$R_{j\gamma} = \frac{3}{2}\int_0^\infty \frac{du}{(u+\lambda+\gamma^2)\Delta(u+\lambda)}. \tag{133}$$

Therefore, using the notation above, the first derivatives are expressed as

$$U_{q_x} = -q_x R_{j\alpha} \tag{134}$$

and

$$U_{q_y} = -q_y R_{j\beta}. \tag{135}$$

For the second derivatives,

$$U_{q_xq_x} = -R_{j\alpha} + \frac{(q_x)^2}{(1+\lambda)^2}(R_{j\alpha}+R_{j\beta}+R_{j\gamma})\left[\frac{1}{\frac{q_x^2}{(1+\lambda)^2}+\frac{q_y^2}{(\beta^2+\lambda)^2}}\right], \tag{136}$$

$$U_{q_yq_y} = -R_{j\beta} + \frac{q_y^2}{(\beta^2+\lambda)^2}(R_{j\alpha}+R_{j\beta}+R_{j\gamma})\left[\frac{1}{\frac{q_x^2}{(1+\lambda)^2}+\frac{q_y^2}{(\beta^2+\lambda)^2}}\right], \tag{137}$$

and

$$U_{q_xq_y} = \frac{q_xq_y}{(1+\lambda)(\beta^2+\lambda)}(R_{j\alpha}+R_{j\beta}+R_{j\gamma})\left[\frac{1}{\frac{q_x^2}{(1+\lambda)^2}+\frac{q_y^2}{(\beta^2+\lambda)^2}}\right] \tag{138}$$

At the relative equilibria, we obtain

$$U_{q_x} = -q_x R_{j\alpha}, \tag{139}$$

$$U_{q_y} = 0, \tag{140}$$

$$U_{q_xq_x} = R_{j\beta} + R_{j\gamma} \tag{141}$$

and

$$U_{q_yq_y} = -R_{j\beta} \tag{142}$$

References

Bellerose, J., Scheeres, D.J.: Periodic orbits in the vicinity of the equilateral points of the restricted full three-body problem. Paper presented at the AAS/AIAA conference, Lake Tahoe, California, AAS-05-295, 7–11 August 2005

Bellerose, J., Scheeres, D.J.: Energy constraints in the restricted full three-body problem: application to binary system 1999 KW4. Paper presented at the AAS/AIAA conference, Sedona, Arizona, AAS-07-224, 28 January–1 February 2006 (2006)

Bellerose, J., Scheeres, D.J.: Periodic orbits in the full two-body problem. Paper presented at the AAS/AIAA conference, Tampa, Florida, AAS-06-169, 22–26 January 2006 (2007a)

Bellerose, J., Scheeres, D.J.: Stability of equilibrium points in the restricted full three body problem. Acta Astronaut. **60**, 141–152 (2007b)

Danby, J.M.A.: Fundamentals of Celestial Mechanics, 2nd edn. Willmann-Bell, VA (1992)
Fahnestock, E.G., Scheeres, D.J.: Simulation of the full two rigid body problem using polyhedral mutual potential and potential derivatives approach. Celestial Mech. Dyn. Astr. **96**(3–4), 317–339 (2006)
Flannery, B.P., Press, W.H., Teukolsky, S.A., Vetterling, W.T.: Numerical Recipies in C: The Art of Scientific Computing, 2nd edn. Cambridge University Press (1996)
Hénon, M.: Exploration Numérique du Problème Restreint II. Annales d' Astrophysique **28**, 992–1007 (1965)
Lee, T., Leok, M., McClamroch, N.H.: Lie group variational integrators for the full body problem in orbital mechanics. Celestial Mech. Dyn. Astr. **98**(2), 121–144 (2007)
Maciejewski, A.J.: Reduction, relative equilibria and potential in the two rigid bodies problem. Celestial Mech. Dyn. Astr. **63**, 1–28 (1995)
Margot, J.-L., Nolan, M.C., Benner, L.A.M., Ostro, S.J., Jurgens, R.F., Giorgini, J.D., Slade, M.A., Campbell, D.B.: Binary asteroids in the near-Earth object population. Science **296**(5572), 1445–1448 (2002)
Scheeres, D.J.: On symmetric central configurations with application to satellite motion about rings. PhD dissertation, The University of Michigan (1992)
Scheeres, D.J.: The restricted Hill four-body problem with applications to the Earth–Moon–Sun system. Celestial Mech. Dyn. Astr. **70**, 75–98 (1998)
Scheeres, D.J.: Stability in the full two body problem. Celestial Mech. Dyn. Astr. **83**, 155–169 (2002)
Scheeres, D.J.: Stability of relative equilibria in the full two-body problem. In: New Trends in Astrodynamics Conference, College Park, Maryland, 2003
Scheeres, D.J.: Relative equilibria for general gravity fields in the sphere-restricted full 2-body problem. Celestial Mech. Dyn. Astr. **94**(3), 317–349 (2006)
Scheeres, D.J.: Rotational fission of contact binary asteroids. Icarus **189**, 370–385 (2007)
Scheeres, D.J., Augenstein, S.: Spacecraft motion about binary asteroids. In: Astrodynamics 2003, Part II, Advances in the Astronautical Sciences Series, vol. 116, pp. 991–1010. Univelt, San Diego (2003)
Scheeres, D.J., Bellerose, J.: The restricted Hill full 4-body problem: application to spacecraft motion about binary asteroids. In: Dellnitz, M., Marsden, J.E. (eds.) Invited paper in a special issue of Dynamical Systems: An International Journal 20(1), pp. 23–44 (2005)
Scheeres, D.J., Williams, B.G., Miller, J.K.: Evaluation of the dynamics environment of an asteroid: application to 433 Eros. J. Guid. Control Dyn. **23**, 466–475 (2000)
Scheeres, D.J., Fahnestock, E.G., Ostro, S.J., Margot, J.-L., Benner, L.A.M., Broschart, S.B., Bellerose, J., Giorgini, J.D., Nolan, M.C., Magri, C., Pravec, P., Scheirich, P., Rose, R., Jurgens, R.F., De Jong, E.M., Suziki, S.: Dynamical configuration of binary near-Earth asteroid (66391) 1999 KW4. Science **314**, 1280–1283 (2006)
Wiggins, S.: Global Bifurcation and Chaos. Springer-Verlag, New York (1998)